

Inflationary predictions in scalar-tensor DBI inflation

Joel M. Weller,^{a,c} Carsten van de Bruck^b and David F. Mota^c

^aInstitute for Theoretical Physics, University of Karlsruhe,
Karlsruhe Institute of Technology, 76128 Karlsruhe, Germany

^bSchool of Mathematics and Statistics, University of Sheffield,
Hounsfield Road, Sheffield S3 7RH, United Kingdom

^cInstitute of Theoretical Astrophysics, University of Oslo,
0315 Oslo, Norway

E-mail: joel.weller@kit.edu, c.vandebruck@sheffield.ac.uk, d.f.mota@astro.uio.no

Abstract. The scalar-tensor Dirac-Born-Infeld (DBI) inflation scenario provides a simple mechanism to reduce the large values of the boost factor associated with single field models with DBI action, whilst still being able to drive 60 e-folds of inflation. Using a slow-roll approach, we obtain an analytical expression for the spectral index of the perturbations and, moreover, determine numerically the regions of the parameter space of the model capable of giving rise to a power spectrum with amplitude and spectral index within the observed bounds. We find that regions that exhibit significant DBI effects throughout the inflationary period can be discarded by virtue of a blue-tilted spectral index, however, there are a number of viable cases — associated with a more red-tilted spectral index — for which the boost factor is initially suppressed by the effect of the coupling between the fields, but increases later to moderate values.

Keywords: inflation, string theory and cosmology

Contents

1	Introduction	1
2	Scalar-tensor DBI inflation	3
3	Analytical treatment of the perturbations	4
3.1	Defining slow-roll parameters	4
3.2	Rewriting the equations of motion	6
3.3	Solving the perturbation equation	8
4	The parameter space of the model	10
5	Conclusions	14
A	Approximating $C_{\chi\chi}$ to first order in slow-roll parameters	17
B	Comparing the exponential and quadratic potentials	19

1 Introduction

Models of inflation based upon the Dirac-Born-Infeld (DBI) action [1, 2] have been much studied in the past few years as an well-motivated example of string cosmology. In this context, the field χ appearing in the DBI Lagrangian is directly related to the radial coordinate of a D3 brane moving in a ‘throat’ region of a compactified space with a speed limit imposed upon its motion. The DBI model is an interesting example of k-inflation [3] (in which the Lagrangian is an arbitrary function of the inflaton and its kinetic term) and has been much studied in this regard. K-inflationary models are noteworthy as the sound speed of the perturbations c_s can be less than 1, which has the effect of forcing the scalar perturbations generated during inflation to freeze-in at scales shorter than the curvature radius [4]. In the DBI model the sound speed is given in terms of the boost factor γ (which plays a role analogous to the Lorentz factor in special relativity) by $c_s^2 = \gamma^{-2}$, so $c_s \rightarrow 0$ as the speed limit is saturated. The original DBI papers concentrated mainly on this ‘relativistic’ regime where γ is large and for which a simple power law inflation solution can be obtained. However, large values of the boost factor are inextricably linked with excessive amounts of non-Gaussianity in the bispectrum of the CMB fluctuations as the non-linearity parameter f_{NL} is proportional to γ^2 in the relativistic case. This leads to an upper bound on the value of the boost factor $\gamma \lesssim 20$, assumed to apply during the first 10 of the last 60 e-folds of inflation which directly affect the CMB radiation. Since the boost factor increases with the number of e-folds of inflation N_{max} , many DBI models with N_{max} sufficiently large predict a high level of non-Gaussianity exceeding current observational bounds (cf. [5, 6] and also [2, 7]). As shown in [8] (cf. [9]) including non-Gaussianity constraints gives an upper bound on the slow-roll parameter. This greatly restricts the number of e-folds of inflation driven by the DBI field.

One should also take into account the theoretical bound on the range of χ , which arises simply because the throat must have finite size (sometimes referred to as the bulk-volume

bound). This is related to the level of tensor perturbations (given in terms of the tensor-to-scalar ratio r) from inflation via the Lyth bound,

$$\Delta\chi = \int_0^{N_{\max}} \left(\frac{r}{8}\right)^{1/2} dN \quad (1.1)$$

which is true for both DBI and slow-roll inflation [7, 10]. This gives an upper bound on r that can be combined with the lower bound derived from the upper bound on γ to place severe constraints on ultra-relativistic DBI models. Similar ideas are used in [11] to derive a series of consistency relations between the principle observable quantities. The problems with observational constraints are made explicit in two detailed numerical studies [5] and [6], which use Monte Carlo methods to compare single field DBI models to recent cosmological observations. Both studies find that the majority of models cannot satisfy the bulk-volume bound; those that remain are slow-roll DBI models with small values of γ .

Several routes have been explored that have a bearing on the problem, in particular the inclusion of other fields in the determinant in the DBI Lagrangian to represent non-radial directions in the throat. With extra degrees of freedom, however, come extra features, in particular non-radial trajectories of the probe brane and non-adiabatic (entropic) fluctuations. These were addressed in [12] (see [13] for recent developments), where the authors introduced ‘spinflation’, accounting for angular momentum in the UV DBI model. Other models involving the angular coordinates of the DBI scenario have been considered in [14, 15] (see also [16–20]). A different type of multi-field model was introduced in [21] in which inflation is driven by two standard DBI fields, each corresponding to a brane with its own sound speed (see also [22], which generalises the assisted inflation scenario for multi-field DBI inflation). Another way in which the standard DBI scenario can be modified is by coupling the DBI field to another scalar field, or, as in [23, 24], to the gravitational term in the action. The effect of coupling in multifield DBI models was considered in [25, 26], focusing on the effect of particle production due the interaction between the ‘inflaton’ brane and trapped branes in the warped throat.¹

In a previous work [27], we studied the consequences of coupling the DBI action to a canonical scalar field φ in a scalar-tensor theory, in order to investigate the effect of an additional scalar field with a non-minimal coupling to gravity in the effective action. We studied a coupling of the form $A = \exp(\beta\varphi)$, arising due to a conformal transformation to the Einstein frame. As in the two-field model described in [28], when the coupling is non-zero, one field acquires a large effective mass, even for couplings of order a tenth of the strength of gravity ($\beta \gtrsim 0.1$). The parameters of the DBI field, which are dependent on the additional scalar field, vary during inflation so that the number of e-folds is extended and the boost factor is decreased (when compared to standard DBI inflation with the same bare parameters). Two potentials for the canonical field were investigated, one with a minimum and one without, yielding similar results for both the background and perturbations, suggesting that the conclusions hold for any choice of potential steep enough to allow φ to closely track the minimum of its effective potential. As discussed above, many DBI models predict a high

¹ Although, like the scalar-tensor DBI inflation model in [27], this scenario involves a DBI action non-minimally coupled to a second field, the motivation and dynamics are very different: for example, in our model the energy density of the φ -field is not negligible (and indeed, is often the dominant contribution to the right-hand side of the Friedmann equation) and varies slowly as the DBI field evolves. These differences notwithstanding, something like this scenario might perhaps provide an promising framework for the phenomenological model discussed here.

level of non-Gaussianity arising due to large values of γ : in the coupled model, the boost factor is reduced, so the level of non-Gaussianity (which is proportional to γ^2 in single field DBI models) may be expected to be smaller than the standard DBI case. If this is the case, the presence of the canonical scalar field may alleviate some of the problems of the DBI inflationary scenario, although we do not address the issue of non-Gaussianity in this paper.

To understand the significance of the model, it is essential to calculate the predicted values of any observable parameters so as to compare with data, however, this is made rather difficult in this case as there are a large number of free parameters capable of affecting the results. In this article, we approach the problem from two fronts. After a brief resumé of the particulars of the scalar-tensor DBI model in Sec. 2, we focus on the ‘slow-roll’ limit of the model in Sec. 3, showing that with a judicious choice of slow-roll parameters, the equations of motion for the perturbations can be made tractable and solved (to first-order) to obtain an expression for the spectral index. In Sec. 4, it is shown that the parameter space can be severely constrained by considering the values of the power spectrum amplitude and the spectral index. The latter measurement in particular rules out a large class of models — those with small values of c_s at horizon crossing, which give rise to a blue-tilted spectrum — so that only scenarios in which DBI characteristics are suppressed at the beginning of the observable period of inflation are allowed. Finally, our results are summarised in Sec. 5

2 Scalar-tensor DBI inflation

In the Einstein frame (cf. [27] for details) the scalar field φ has a canonical kinetic term and does not couple explicitly to the gravity sector, so the action for the model takes the form

$$S = \int d^4x \sqrt{-g} \left[\frac{1}{2}R + \mathcal{L}_\varphi + \mathcal{L}_{\text{DBI}} \right], \quad (2.1)$$

where

$$\mathcal{L}_\varphi = -\frac{1}{2}g^{\mu\nu} \varphi_{,\mu} \varphi_{,\nu} - U(\varphi), \quad (2.2)$$

$$\mathcal{L}_{\text{DBI}} = A^4(\varphi) \left[f^{-1}(\chi) (1 - \gamma^{-1}) - V(\chi) \right]. \quad (2.3)$$

$V(\chi) = \frac{1}{2}m^2\chi^2$ and $U(\varphi)$ are the potentials for the DBI field χ and the canonical scalar field φ respectively. Two forms for $U(\varphi)$ were investigated in [27], one of an exponential form

$$U(\varphi) = U_0 \exp(-\eta\varphi), \quad (2.4)$$

and another, quadratic potential $U(\varphi) = U_0(\varphi - \eta)^2$ with a minimum at $\varphi = \eta$. It was found that when the coupling between the fields was non-zero, both potentials led to extremely similar behaviour, so for simplicity the exponential potential (2.4) will be used throughout the body of the article, and the results of the numerical analysis for the quadratic potential will be summarised in Appendix B.

$f(\chi)$ is the warp factor of the DBI field, a measure of the geometry of the throat region of the compactified space in which the brane moves. As in [27], in the following the ‘mass-gap solution’ [2, 29]

$$f(\chi) = \frac{\lambda}{(\mu^2 + \chi^2)^2}, \quad (2.5)$$

will be used, which exhibits the salient features of a capped throat with a cutoff at the IR end. The presence of the mass scale μ (which must be subplanckian in order to get a warped

throat) suppresses the DBI effects as the χ -field moves to smaller values. Generally, the smaller the value of μ , the larger the γ factor can become during the inflationary period and the more e-folds one observes.

The boost factor γ appearing in (2.3) is modified by a φ -dependent factor of the conformal coupling $A(\varphi)$ compared to the standard DBI model by a factor, so that

$$\gamma = \frac{1}{\sqrt{1 - A^{-2} f \dot{\chi}^2}}, \quad (2.6)$$

where the dot indicates a derivative with respect to cosmic time. (Here, as throughout this article, a flat Friedmann-Robertson-Walker metric is assumed: $ds^2 = -dt^2 + a^2(t)\delta_{ij}dx^i dx^j$.) The conformal coupling $A(\varphi)$ is given by

$$A(\varphi) = \exp(\beta\varphi), \quad (2.7)$$

in terms of the constant β .

The dynamical evolution of the system is determined by the background equations of motion for the homogeneous fields

$$\ddot{\chi} + 3H\gamma^{-2}\dot{\chi} + \frac{1}{2}A^2\frac{f_{\chi}}{f^2}(1 - 3\gamma^{-2} + 2\gamma^{-3}) + A^2\gamma^{-3}V_{\chi} = -\beta\dot{\chi}\dot{\varphi}(3\gamma^{-2} - 1), \quad (2.8)$$

$$\ddot{\varphi} + 3H\dot{\varphi} + U_{\varphi} = \beta A^4 [f^{-1}(4 - 3\gamma^{-1} - \gamma) - 4V], \quad (2.9)$$

where $f_{\chi} = \partial f/\partial\chi$ and $V_{\chi} = \partial V/\partial\chi$, together with the Friedmann equations

$$3H^2 = \frac{1}{2}\dot{\varphi}^2 + U + A^4 [f^{-1}(\gamma - 1) + V], \quad (2.10)$$

$$-2\dot{H} = \dot{\varphi}^2 + \gamma A^2 \dot{\chi}^2. \quad (2.11)$$

3 Analytical treatment of the perturbations

In [27], the equations of motion for the first-order perturbations and the perturbed Einstein equations were derived in full and solved numerically. As was expected, the perturbations of the DBI field were found to propagate with a sound speed defined by $c_s^2 = \gamma^{-2}$; however, many extra terms appear involving factors of c_s , the coupling β and derivatives of the warp factor f , which render the full equations intractable. In this section, we derive approximations for the background dynamics in the scenario in which the φ -field is trapped in the minimum of its effective potential. It is shown that in this case one can rewrite the perturbation equations in terms of slow-roll parameters and hence obtain an expression for the spectral index of scalar perturbations that is in excellent agreement with the numerical analysis in the following section.

3.1 Defining slow-roll parameters

As was shown in [27], in the coupled case with $\beta > 0$, the situation is simplified considerably as the extra mass term on the right-hand side of (2.9) means that the effective potential can have a minimum value at which the field value $\varphi = \varphi_{\min}$ satisfies,

$$\left. \frac{dU}{d\varphi} \right|_{\varphi=\varphi_{\min}} - \beta e^{4\beta\varphi_{\min}} T_{DBI}^b = 0, \quad (3.1)$$

where $T_{DBI}^b = f^{-1}(4 - \gamma - 3\gamma^{-1}) - 4V \approx -4V$ is the trace of the ‘bare’ DBI stress-energy tensor and the φ dependence of $A(\varphi)$ has been written explicitly using (2.7). With the exponential potential (2.4) the condition for the minimum in this case is

$$U \simeq \frac{4\beta}{\eta} A^4 V, \quad (3.2)$$

so the minimum is given by the logarithmic function

$$\varphi_{\min} = \frac{1}{4\beta + \eta} \log \left(\frac{\eta U_0}{4\beta V} \right), \quad (3.3)$$

(cf. [28], in which a similar condition is obtained for two coupled scalar fields). Even for relatively small values of the coupling β , the φ -field is forced into this minimum, the position of which changes as the χ -field evolves as²

$$\dot{\varphi} = - \left(1 + \frac{4\beta}{\eta} \right)^{-1} \left(\frac{V_\chi}{V} \right) \frac{\dot{\chi}}{\eta}, \quad (3.4)$$

so that the second Friedmann equation can be approximated as

$$-2\dot{H} \simeq A^2 \gamma \dot{\chi}^2. \quad (3.5)$$

When the coupling between the two fields is switched on, the DBI equation of motion is dominated by the Hubble friction and potential terms (we have checked this numerically and found it to be an excellent approximation). Thus (2.8) can be approximated by the slow-roll equation

$$3H\gamma^{-2}\dot{\chi} + A^2\gamma^{-3}V_\chi \simeq 0, \quad (3.6)$$

i.e.

$$\dot{\chi} \simeq -\frac{A^2 V_\chi}{3H\gamma}. \quad (3.7)$$

Finally, as the contribution of the kinetic terms of the fields in (2.10) is negligible, one can rewrite the Friedmann equation as

$$3H^2 \simeq \left(1 + \frac{4\beta}{\eta} \right) A^4 V, \quad (3.8)$$

using (3.2). We are now in a position to define the first slow roll parameter $\epsilon = -\dot{H}/H^2$, which using (3.7), can be written

$$\epsilon \simeq \frac{1}{2A^2\gamma} \left(1 + \frac{4\beta}{\eta} \right)^{-2} \left(\frac{V_\chi}{V} \right)^2. \quad (3.9)$$

We can use this expression to obtain an expression for $\dot{\varphi}$ in terms of ϵ . Substituting (3.7) into (3.4) gives

$$\dot{\varphi} \simeq \frac{2}{\eta} H \epsilon. \quad (3.10)$$

² This corrects a minor error in eqn. (3.31) of [27].

The rate of change of the slow-roll parameters should be second order in ϵ . Differentiating (3.9) with respect to time gives

$$\begin{aligned}
\frac{\dot{\epsilon}}{2H\epsilon} &\simeq \frac{1}{2H\epsilon} \left[\left(\frac{\dot{c}_s}{c_s} - 2\beta\dot{\varphi} \right) \epsilon + \frac{1}{A^2\gamma} \left(1 + \frac{4\beta}{\eta} \right)^{-2} \left(\frac{V_\chi}{V} \right) \left(\frac{V_{\chi\chi}}{V} - \frac{V_\chi^2}{V^2} \right) \dot{\chi} \right], \\
&\simeq \frac{\dot{c}_s}{2Hc_s} - \frac{2\beta}{\eta} \epsilon - \frac{1}{A^2\gamma} \left(1 + \frac{4\beta}{\eta} \right)^{-1} \left(\frac{V_{\chi\chi}}{V} - \frac{V_\chi^2}{V^2} \right), \\
&\simeq \frac{\dot{c}_s}{2Hc_s} - \frac{1}{A^2\gamma} \left(1 + \frac{4\beta}{\eta} \right)^{-1} \frac{V_{\chi\chi}}{V} + 2 \left(1 + \frac{3\beta}{\eta} \right) \epsilon, \\
&= \frac{1}{2}s - \delta + 2 \left(1 + \frac{3\beta}{\eta} \right) \epsilon,
\end{aligned} \tag{3.11}$$

where the slow-roll parameters δ and s are defined as follows

$$\delta \equiv \frac{1}{A^2\gamma} \left(1 + \frac{4\beta}{\eta} \right)^{-1} \frac{V_{\chi\chi}}{V}, \quad s \equiv \frac{\dot{c}_s}{Hc_s}. \tag{3.12}$$

δ is the equivalent of the commonly used η parameter and s is a measure of the rate of change of the sound speed, which matches the definition used in the DBI literature (cf. [7]). Note, that s has an implicit dependence of $A(\varphi)$ through the definition of γ in (2.6).

3.2 Rewriting the equations of motion

It was demonstrated in [27] that when the φ -field is trapped in the minimum of its effective potential, the effect of the perturbations $\delta\varphi(t, \mathbf{x})$ is negligible and the coupled DBI model is effectively a single field system. The first-order perturbations can then be well-described by the Fourier components of the single variable $u = r_\chi Q_\chi$. Here r_χ is the combination of background quantities

$$r_\chi = aAc_s^{-3/2} \tag{3.13}$$

and $Q_\chi \equiv \delta\chi + \frac{\dot{\chi}}{H}\Psi$ is the gauge-invariant Mukhanov-Sasaki variable constructed from the DBI field perturbation $\delta\chi$ and the metric perturbation Ψ . The perturbation equation in conformal time τ (with $' = d/d\tau$) is therefore [cf. eqn. (4.22) in [27]]

$$u_k'' + \left[k^2 c_s^2 + a^2 C_{\chi\chi} - \frac{r_\chi''}{r_\chi} \right] u_k = 0, \tag{3.14}$$

with

$$\begin{aligned}
C_{\chi\chi} &= \frac{A^4 \dot{\chi}}{H} \frac{f_\chi}{f^2} (1 - c_s)^2 - \left[\frac{f_\chi}{f} - \frac{A^2 \dot{\chi}}{Hc_s} \right] \frac{\dot{c}_s}{c_s} \dot{\chi} - \frac{1}{2} c_s f_\chi A^{-4} \dot{\chi}^2 V_{T,\chi} + \\
&+ \frac{1}{2} A^2 (1 - c_s)^2 \left[c_s \left(\frac{f_\chi}{f^2} \right)_{,\chi} + (1 + c_s) f^{-1} \left(\frac{f_\chi}{f} \right)_{,\chi} \right] + \frac{3}{2} A^2 \dot{\chi}^2 c_s^{-1} (1 + c_s^2) - \\
&- A^4 c_s^{-2} \frac{\dot{\chi}^4}{2H^2} - A^2 c_s^{-1} (1 + c_s^2) \frac{\dot{\chi}^2 \dot{\varphi}^2}{4H^2} + \frac{\dot{\chi} V_{T,\chi}}{H} (1 + c_s^2) + c_s^3 A^{-2} V_{T,\chi\chi}.
\end{aligned} \tag{3.15}$$

Analysing each term in (3.15) separately, one can rewrite the expression in terms of the slow-roll parameters ϵ , δ and s as

$$C_{\chi\chi} \simeq 3H^2 \left(\delta - s - 2\epsilon \left[1 + \frac{\beta}{\eta} (1 - c_s^2) \right] \right). \tag{3.16}$$

The interested reader is directed to Appendix A for full details of the derivation of this equation. Differentiating r_χ with respect to conformal time gives

$$\begin{aligned}\frac{r'_\chi}{r_\chi} &= \mathcal{H} \left(1 + \frac{\beta\varphi'}{\mathcal{H}} - \frac{3}{2} \frac{c'_s}{c_s \mathcal{H}} \right), \\ &\simeq \mathcal{H} \left(1 + \frac{2\beta}{\eta} \epsilon - \frac{3}{2} s \right).\end{aligned}\tag{3.17}$$

Differentiating again (again assuming the derivatives of ϵ and s are second order) yields

$$\begin{aligned}\frac{r''_\chi}{r_\chi} &= \left(\frac{r'_\chi}{r_\chi} \right)' + \left(\frac{r'_\chi}{r_\chi} \right)^2, \\ &\simeq \mathcal{H}' \left(1 + \frac{2\beta}{\eta} \epsilon - \frac{3}{2} s \right) + \mathcal{H}^2 \left(1 + \frac{4\beta}{\eta} \epsilon - 3s \right), \\ &\simeq \mathcal{H}^2 \left[(1 - \epsilon) \left(1 + \frac{2\beta}{\eta} \epsilon - \frac{3}{2} s \right) + \left(1 + \frac{4\beta}{\eta} \epsilon - 3s \right) \right], \\ &\simeq \mathcal{H}^2 \left[2 - \frac{9}{2} s - \left(1 - \frac{6\beta}{\eta} \right) \epsilon \right],\end{aligned}\tag{3.18}$$

using $\mathcal{H}' = \mathcal{H}^2(1 - \epsilon)$. Combining (3.16) and (3.18) means the combination that appears in the equation of motion can be simplified to

$$a^2 C_{\chi\chi} - \frac{r''_\chi}{r_\chi} \simeq -\mathcal{H}^2 \left[2 - \frac{3}{2} s - 3\delta + \left(5 + \frac{6\beta}{\eta} (2 - c_s^2) \right) \epsilon \right].\tag{3.19}$$

Defining the background variable z by

$$z = \frac{a\sqrt{p+\rho}}{c_s H} = \frac{a\sqrt{-2\dot{H}}}{c_s H} = a\gamma\sqrt{2\epsilon},\tag{3.20}$$

one can show [using (3.11) and (3.19)] that

$$a^2 C_{\chi\chi} - \frac{r''_\chi}{r_\chi} \simeq -\frac{z''}{z} + \frac{6\beta}{\eta} \epsilon \mathcal{H}^2 (1 + c_s^2),\tag{3.21}$$

which is correct to first order in ϵ , s and δ . The first term on the RHS appears (without the factor of A in the definition of z) in single field k-inflation models [4]. Alone, this would indicate that the combination $|u_k/z|$ becomes approximately constant for small k ; the small correction proportional to $(1+c_s^2)$ arises due to the fact that (3.14) is an approximation to the full, two-field model given by eqns (4.21) and (4.22) in [27]. The correction is proportional to ϵ and thus subdominant to z''/z in the mass term: this can be seen when comparing the size of the terms in the full equations (when evaluated numerically, as in the following section) and in many cases the correction is not too much larger than the terms proportional to the scalar field perturbations that have been neglected in (3.14). Thus, to a good approximation, we can neglect the second term in (3.21). In this case the evolution of u_k is determined by the (approximate) equation

$$u''_k + \left[k^2 c_s^2 - \frac{z''}{z} \right] u_k \simeq 0,\tag{3.22}$$

or, in terms of the slow-roll parameters

$$u''_k + \left(k^2 c_s^2 - \mathcal{H}^2 \left[2 - \frac{3}{2} s - 3\delta + \left(5 + \frac{18\beta}{\eta} \right) \epsilon \right] \right) u_k \simeq 0.\tag{3.23}$$

The comoving curvature perturbation of the full two-field system is given by eqn. (4.27) in [27] as

$$\mathcal{R} = \frac{H}{(-2\dot{H})} [\dot{\varphi}Q_\varphi + A^2\gamma\dot{\chi}Q_\chi].$$

where Q_χ and Q_φ are the gauge-invariant Mukhanov-Sasaki variables for the perturbations of the χ and φ fields respectively. Neglecting the Q_φ term and using (3.20), one gets

$$\mathcal{R} \simeq \frac{A\gamma^{1/2}}{\sqrt{2\epsilon}}Q_\chi = \frac{u_k}{z},$$

as $Q_\chi = u_k/r_\chi = \sqrt{2\epsilon}c_s^{1/2}A^{-1}u_k/z$. The power spectrum is given by

$$\mathcal{P}_\mathcal{R} \simeq \frac{k^3}{2\pi^2} \left| \frac{u_k}{z} \right|^2. \quad (3.24)$$

3.3 Solving the perturbation equation

As in the standard slow-roll case, eqn. (3.23) admits a solution in terms of Hankel functions. However, to account for the fact that c_s is not constant we follow the approach of [30] and rewrite the equation using the time variable

$$y \equiv \frac{c_s k}{aH} = \frac{c_s k}{\mathcal{H}}, \quad (3.25)$$

so $y = 1$ at sound horizon crossing. For a related approach, see [9, 31]. The derivatives of u_k can be rewritten in terms of the slow-roll parameters as

$$\frac{du_k}{d\tau} = -c_s k(1 - \epsilon - s) \frac{du_k}{dy} \quad (3.26)$$

(using $\mathcal{H}' = \mathcal{H}^2(1 - \epsilon)$) and

$$\frac{d^2u_k}{d\tau^2} = \mathcal{H}^2 \left[(1 - \epsilon - s)^2 y^2 \frac{d^2u_k}{dy^2} - s(1 - \epsilon - s)y \frac{du_k}{dy} \right]. \quad (3.27)$$

Substituting these expressions into (3.19) gives

$$(1 - \epsilon - s)^2 y^2 \frac{d^2u_k}{dy^2} - s(1 - \epsilon - s)y \frac{du_k}{dy} + \left[y^2 - 2 + \frac{3}{2}s + 3\delta - \epsilon \left(5 + \frac{18\beta}{\eta} \right) \right] u_k = 0, \quad (3.28)$$

which can be written in the form

$$y^2 \frac{d^2u_k}{dy^2} + (1 - 2p)y \frac{du_k}{dy} + [\ell^2 y^2 + p^2 - \nu^2] u_k = 0 \quad (3.29)$$

with

$$p = \frac{1}{2}(1 + s), \quad (3.30)$$

$$\ell = (1 - \epsilon - s)^{-1}, \quad (3.31)$$

$$\nu = \frac{3}{2} + s - \delta + 3\epsilon \left(1 + \frac{2\beta}{\eta} \right). \quad (3.32)$$

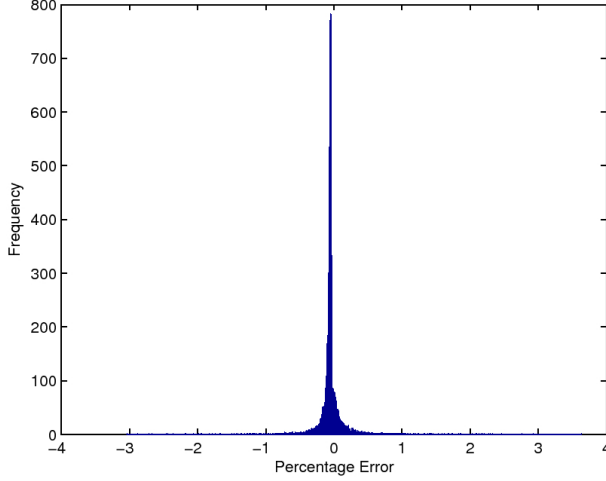


Figure 1. For comparison between the numerical and analytical predictions, the value of n_s was estimated using (3.38) for 13056 parameter sets with $\mathcal{P}_{\mathcal{R}}$ in the observed range. The histogram shows the percentage error between the estimated result and that obtained from numerical integration of the perturbation equations. It can be seen that the vast majority of the n_s -values estimated using (3.38) differ less than 1% from the calculated value.

The solution of eqn. (3.29) is $u_k = z^p \zeta_\nu(\ell z)$ where ζ_ν is a Bessel function of order ν [32]. The general solution is

$$u_k(y) = y^{\frac{1}{2} + \frac{s}{2}} \left[c_1 H_\nu^{(1)}(\ell y) + c_2 H_\nu^{(2)}(\ell y) \right] \quad (3.33)$$

using Hankel functions of the first and second kind. Comparing with the short wavelength solution $u_k(y \gg 1) \approx e^{-kc_s \tau} / \sqrt{2c_s k}$ means $c_2 = 0$ and $c_1 = \sqrt{\pi/4kc_s}$ so (up to a phase factor)

$$u_k(y) = \frac{1}{2} \sqrt{\frac{\pi}{c_s k}} \sqrt{\frac{y}{1 - \epsilon - s}} H_\nu^{(1)} \left(\frac{y}{1 - \epsilon - s} \right). \quad (3.34)$$

In the long wavelength limit $H_\nu^{(1)}(y \ll 1) \sim \sqrt{\frac{2}{\pi}} e^{-i\pi/2} 2^{\nu - \frac{3}{2}} \frac{\Gamma(\nu)}{\Gamma(\frac{3}{2})} y^{-\nu}$, so

$$|u_k(y)| \sim 2^{\nu - \frac{3}{2}} \frac{\Gamma(\nu)}{\Gamma(\frac{3}{2})} (1 - \epsilon - s)^{\nu - \frac{1}{2}} \frac{y^{\frac{1}{2} - \nu}}{\sqrt{2c_s k}}. \quad (3.35)$$

Thus, from (3.24) we find

$$\mathcal{P}_{\mathcal{R}}^{1/2} \simeq \frac{\sqrt{2c_s k} H y}{2^{3/2} \pi \sqrt{c_s \epsilon}} |u_k|. \quad (3.36)$$

Defining $\mathcal{V}(\nu) = 2^{\nu - 3} (1 - \epsilon - s)^{\nu - \frac{1}{2}} \Gamma(\nu) / \Gamma(\frac{3}{2})$ and using (3.35) this can be written

$$\mathcal{P}_{\mathcal{R}}^{1/2} \simeq \left(\frac{\mathcal{V}(\nu)}{\pi} \right) \frac{H}{\sqrt{c_s \epsilon}} y^{\frac{3}{2} - \nu}, \quad (3.37)$$

so the spectral index is

$$\begin{aligned} n_s &= 1 + (3 - 2\nu), \\ &= 1 - 2s + 2\delta - 6\epsilon \left(1 + \frac{2\beta}{\eta} \right). \end{aligned} \quad (3.38)$$

This estimate compares extremely well (significantly less than 1% error in most cases) with the value obtained by solving the perturbation equations numerically described in the following section. The comparison is illustrated in Fig. 1. Note that, as β/η is not necessarily less than one, the terms in $\epsilon\beta/\eta$ are of the same order as the other slow-roll parameters and should not be neglected in (3.38). In fact, numerically, we find that dropping these terms shifts the value of the spectral index by a large factor of roughly 5-10%. Comparing (3.38) with the corresponding equation in single field slow-roll $n_s = 1 + 2\delta - 6\epsilon$ [33] and the single field DBI case³ $n_s = 1 - 2s + 2\delta - 6\epsilon$ [7], it can be seen that the standard expression is recovered when the coupling is small.

In Fig. 1, (3.38) was evaluated at sound horizon crossing $kc_s = aH$ i.e $y = 1$. As the definitions of ϵ and δ explicitly include factors of $A = e^{\beta\varphi}$, it is useful to check to what extent the power spectrum and the spectral index depends on the evolution of the fields. The sound horizon crossing formalism can be expressed by the condition

$$\frac{d}{dy} \left(\frac{H}{\sqrt{c_s\epsilon}} y^{\frac{3}{2}-\nu} \right) = 0, \quad (3.39)$$

[30] which ensures that the that the expression for $\mathcal{P}_{\mathcal{R}}^{1/2}$ is independent of y and can safely be evaluated at the sound horizon crossing $y = 1$. Following [30], we can generalise this condition. Observing that

$$\frac{d}{dy} = -\frac{1}{yH(1-\epsilon-s)} \frac{d}{dt}, \quad (3.40)$$

it follows that

$$\begin{aligned} y \frac{d}{dy} \left(\frac{H}{\sqrt{c_s\epsilon}} y^{\frac{3}{2}-\nu} \right) &= \left[\left(\frac{3}{2} - \nu \right) \frac{H}{\sqrt{c_s\epsilon}} - \frac{1}{H(1-\epsilon-s)} \frac{d}{dt} \left(\frac{H}{\sqrt{c_s\epsilon}} \right) \right] y^{\frac{3}{2}-\nu}, \\ &\simeq \left[\frac{3}{2} - \nu + \frac{\epsilon + \frac{1}{2}s + \dot{\epsilon}/(2\epsilon H)}{1-\epsilon-s} \right] \frac{H}{\sqrt{c_s\epsilon}} y^{\frac{3}{2}-\nu}, \\ \Rightarrow \frac{d}{d \log(y)} \log \left(\frac{H}{\sqrt{c_s\epsilon}} y^{\frac{3}{2}-\nu} \right) &\simeq \frac{3}{2} - \nu + \frac{s - \delta + 3\epsilon \left(1 + \frac{2\beta}{\eta} \right)}{1-\epsilon-s}. \end{aligned} \quad (3.41)$$

Inserting the value of ν in (3.32), obtained by neglecting the two-field correction to the u_k mass term, it can be seen that (to first order in the slow-roll parameters) the expression for the power spectrum is independent of the y -value at which it is evaluated. This justifies our assumption that we can evaluate the power spectrum at sound horizon crossing.

4 The parameter space of the model

The scalar-tensor DBI inflation model has thus far been investigated in detail in scenarios in which the φ -field is in the minimum of its effective potential, in order to specify uniquely the initial conditions and to neglect short-term effects due to the field oscillating as it reaches the minimum⁴. Even in this restricted case, the inflationary dynamics are determined by six parameters: the coupling β , the t'Hooft coupling λ and the cutoff scale μ in the DBI warp

³ This result is quoted [cf. eqn. (40) in [7]] in the form $n_s = -2\epsilon - \tilde{\eta} - s$ where $\tilde{\eta} = \dot{\epsilon}/(H\epsilon)$. However, one can see from (3.11) that in the limit $\beta \rightarrow 0$, $\tilde{\eta} = s - 2\delta + 4\epsilon$, which gives the stated result.

⁴ In this case the initial value of the χ -field is of less importance as, for a given set of parameters, the system proceeds along a single trajectory in field space. The anisotropies in the CMB radiation are affected

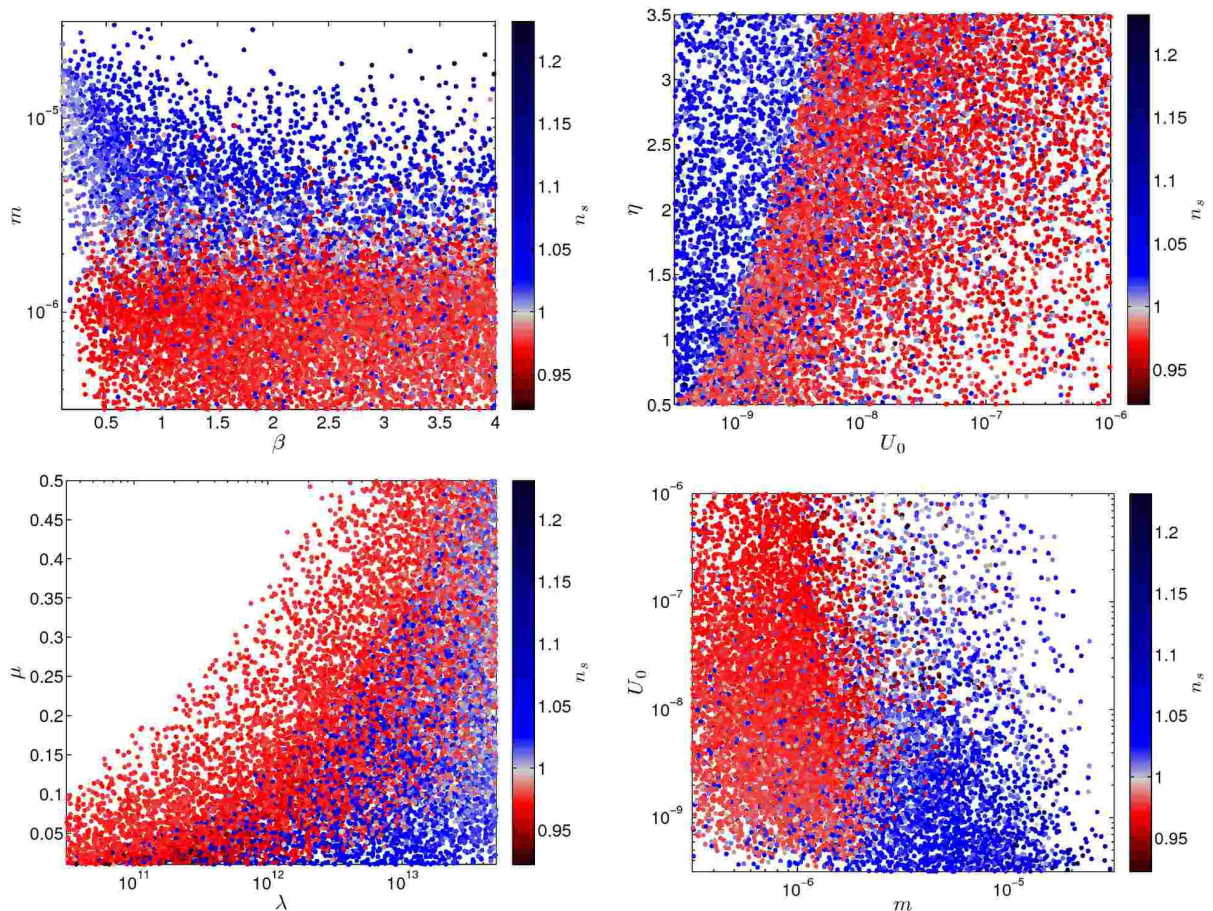


Figure 2. Spectral index plots for the ‘better’ set (with power spectrum amplitude within observational limits) for the exponential potential, colour-coded according to the value of n_s . Upper-left panel: the $\beta - \log_{10} m$ plane; upper-right panel: the $\log_{10} U_0 - \eta$ plane; lower-left panel: $\log_{10} \lambda - \mu$ plane; lower-right panel: $\log_{10} m - \log_{10} U_0$ plane.

factor, the mass term in the quadratic potential of the DBI field m and the two constants in the φ -field potential U_0 and η . It is possible to understand the importance of these different parameters by keeping five fixed and varying one (as in figs. 5, 7 and 9 in [27]). However, this only gives a limited view of the effect of changing a particular parameter on the observations. To improve upon this, one can perform multiple runs using random sets of parameters from within a given range to compare the resulting values of the power spectrum amplitude and spectral index with observations. In the following, the results of such an analysis are analysed for the exponential potential. The quadratic potential yielded similar results: these are discussed in Appendix B.

by the range of scales (around 4 orders of magnitude or 10 e-folds) that cross the curvature horizon roughly 55 e-folds before the end of inflation. Thus, only the behaviour of the system in the last 60-70 e-folds of inflation is needed to compare with observations and we are free to choose values χ_{ini} that allow an inflationary period of sufficient duration, bearing in mind string theory constraints on the maximum length of the throat (cf. [5, 7]) that mean $\chi_{\text{ini}} \lesssim \mathcal{O}(1)$ in Planck units. In all of the examples presented here, $\chi_{\text{ini}} = 1.5$ has been used.

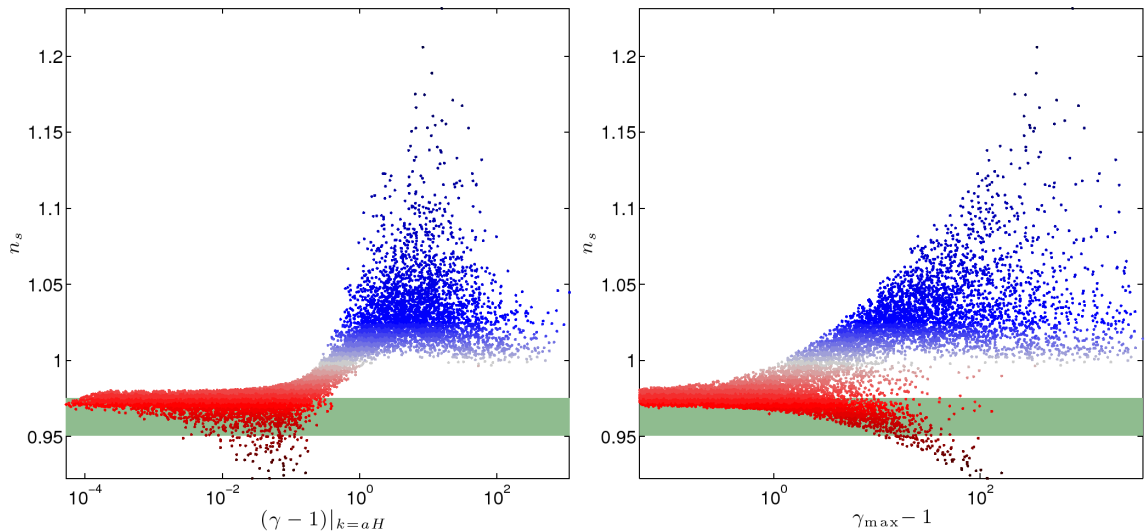


Figure 3. Correlations between the spectral index and the DBI boost factor for the exponential potential (Note the log scale on the x-axis.) The left panels show $(\gamma - 1)$ (calculated at $k_{\text{pivot}} = aH$) against n_s , with the green region indicating the observational limits on the spectral index. The right-panels show the correlation between $(\gamma_{\text{max}} - 1)$ and n_s . (Points are colour-coded according to the value of n_s , for easy comparison with the parameter-space plots in figs. 2).

The parameter ranges⁵ used in the run with the exponential potential were

$$\beta \in [0.1, 4], \lambda \in [10^{10.5}, 5 \times 10^{13}], m \in [10^{-6.5}, 10^{-4.5}], \\ U_0 \in [10^{-9.5}, 10^{-6}], \mu \in [0.01, 0.5], \eta \in [0.5, 3.5]. \quad (4.1)$$

5 million parameter sets were investigated, of which 2,231,657 (44.6%) satisfied the criteria for the background evolution⁶. Most of the points rejected at this stage (60%) yielded too few e-folds, with the majority of the remainder exhibiting slow-roll in χ (38%). With the range of parameters given above, the volume of the parameter space was rather large, which meant that only a relatively small number of parameter sets (13063) were found that gave rise to a power spectrum amplitude within the observed range⁷. This shall be referred to

⁵ These ranges were based on preliminary tests in which it was found that a large range of values of the parameters U_0 and λ (and to some extent, m) gave rise to a power spectrum amplitude within observable limits. Only non-zero couplings $\beta > 0$ were considered so as to ensure the presence of a minimum for the φ -field, in which case there is a unique trajectory in field space for a given set of parameters.

⁶ The two most important criteria are that there should be a sufficient amount of inflation to solve the horizon and flatness problems and that the maximum value of γ (considered over the entire run) should be greater than 1. The latter case, of course, is far from unphysical as it corresponds to a two-field model with slowly rolling coupled scalar fields. However, in this section we focus on deviations from the standard scenario so exclude these models to focus on the more unusual phenomenology associated with the DBI field.

⁷ This can be understood by considering the analogous process in the single-field case, in which the power spectrum amplitude P_{amp} is proportional to the squared mass of the field. Increasing the volume of the parameter space (either by extending the range of mass values tested or increasing the dimension of the parameter space) means that the number of cases that *do not* give rise to the observational value of P_{amp} is vastly increased.

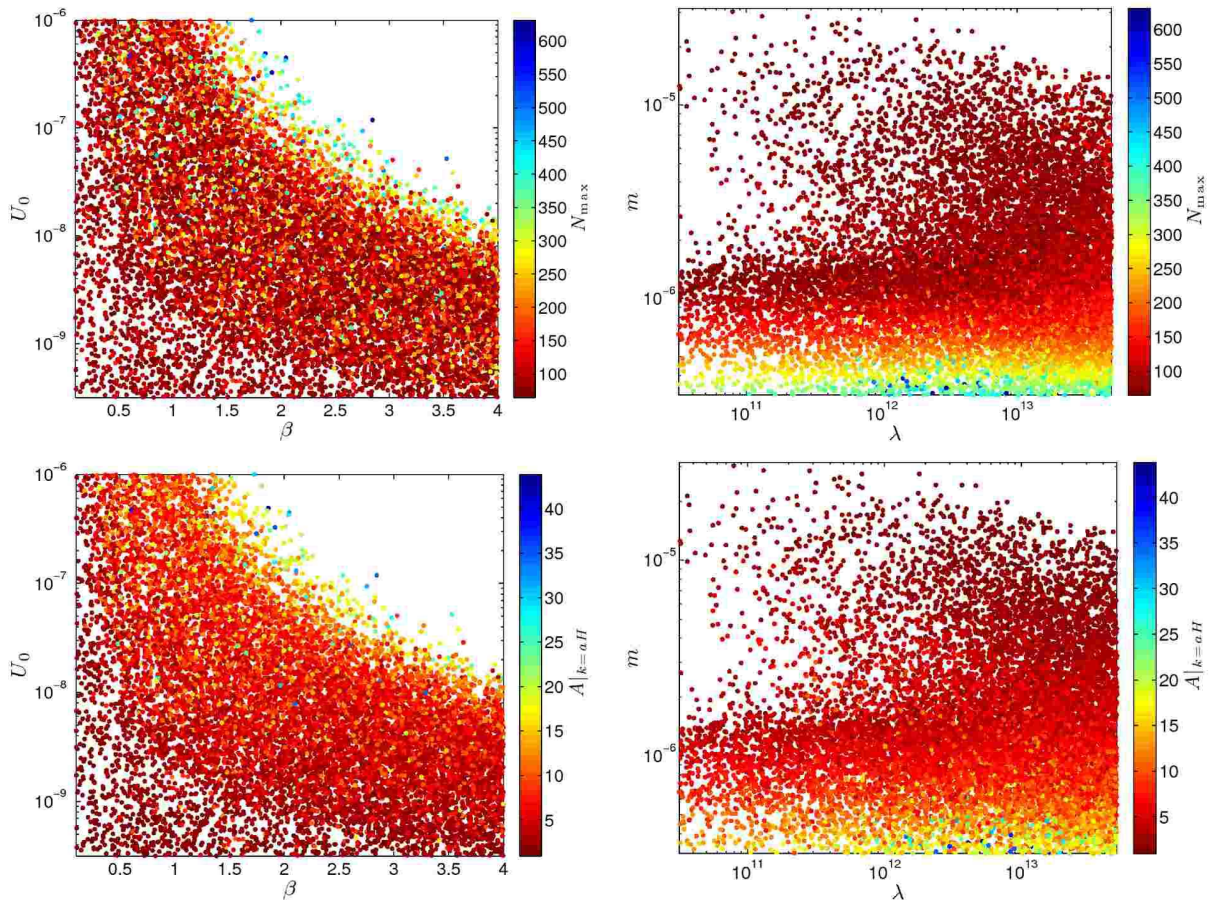


Figure 4. The $\beta - \log_{10} U_0$ (left column) and $\log_{10} \lambda - \log_{10} m$ (right column) planes for the ‘better set’ for the exponential potential. The upper plots are colour-coded according to the number of e-folds in the run N_{\max} and the lower plots according to the value of A at $k_{\text{pivot}} = aH$.

as the ‘better’ set. Similarly, the ‘best’ set for which both the power spectrum and spectral index were within observational limits yielded 3834 points.

Except for some runs with the coupling β very close to zero, no distinct region of the parameter space was excluded by discounting the parameter sets that did not satisfy the criteria for the background evolution (i.e. gave rise to an extremely short inflationary stage or standard slow-roll models). The relatively large range of parameters considered means that the calculated value of the power spectrum amplitude varies over several orders of magnitude with a strong dependence on the mass scale of the DBI field (as is to be expected since it is the perturbations of the DBI field that are the dominant contribution to the curvature perturbation). Larger values of the φ -field potential, corresponding to small η and large U_0 , increase the Hubble parameter and also give rise to larger values of P_{amp} .

Focusing on the ‘better set’ of runs with P_{amp} within observational limits, one can see in fig. 2 that the parameter space is significantly constrained compared to the ‘good set’, although the range of values of the spectral index n_s is quite large. There appear to be two overlapping regions in the plots in fig. 2. The light blue points with $n_s \approx 0.97$ make up the bulk of the ‘best set’ (shown in more detail in fig. 5) and have $\gamma \simeq 1$ as the pivot

scale crosses the horizon, so the spectral index is similar to that in slow-roll models as DBI corrections are minimal. To illustrate more clearly the qualitative difference in the properties of the background runs that give rise to the distinct regions in fig. 2, correlations between the boost factor and n_s are shown in fig. 3. As γ is a dynamical quantity that increases to a maximum as inflation proceeds, two views are shown: in the left panel, the value taken when the pivot mode leaves the horizon $(\gamma - 1)|_{k_{\text{pivot}}=aH}$ (corresponding to $N = 55$) and the maximum value obtained throughout the background run $(\gamma_{\text{max}} - 1)$ (right panel). As the value of n_s shown on the vertical axis is a constant property for a given run, the points can be thought of moving horizontally between the left panel and the right as inflation proceeds. It can be seen that the runs which do exhibit significant DBI characteristics (as indicated by $\gamma_{\text{max}} \gtrsim 100$ in the right-panel plot) are precisely those with larger values of the boost factor at horizon crossing that are excluded by virtue of a blue-tilted spectral index. This is, however, not to say that there are no viable scenarios that exhibit DBI characteristics as some of the darker blue points — which, as can be seen by comparing figs. 2 and 3, are associated with smaller values of λ and μ , and a DBI mass scale $m \sim \mathcal{O}(10^{-6})$ — correspond to runs in which the boost factor increases from a very tiny value to $\gamma_{\text{max}} \sim \mathcal{O}(10)$. In both cases, deviations from the quasi-slow-roll solutions with $\gamma - 1 \ll 1$ throughout the background evolution give rise to a corresponding shift in the resulting spectral index of the perturbations, leading to either a blue-tilted (for the points corresponding to solutions bearing close resemblance to standard DBI models) or a more red-tilted spectrum (for the points in which DBI characteristics are suppressed by the presence of the second field).

The parameters λ and m strongly affect the other background quantities: the duration of inflation N_{max} and the coupling A (measured at $k_{\text{pivot}} = aH$). The models with $A \gtrsim 10$ (and P_{amp} in the observed range) have small m to compensate (cf. fig. 4). In a similar way to the case shown in fig. 9 of [27] these models can exhibit slow-roll inflation in χ so that N_{max} is very large. As might be expected, models with large A have $\beta > 1$; the left column of fig. 4 shows a noticeable correlation between β and $\log_{10} U_0$ for these models.

Looking at the ‘best’ set for this model, with both n_s and P_{amp} within observational limits (fig. 5) it can be seen that most of the allowed models have very similar properties, with the boost factor γ at horizon crossing deviating only slightly from 1 and rising to values less than $\mathcal{O}(10)$. The allowed range of the DBI mass m is relatively small (one order of magnitude) compared to U_0 and a large range of β values are compatible with observations. The plots showing the $\beta - \log_{10} U_0$ and $\log_{10} U_0 - \eta$ display clear structure, favouring larger values for the potential of the φ -field (when β is not large) than in typical slow-roll scenarios, further emphasising the non-dynamical role of the field. The bottom-right plot, showing the $\log_{10} \lambda - \mu$ plane is also tightly constrained, with values that lead to large $f(\chi)$ excluded. As in the standard DBI scenario, a larger value of the warp factor is related to a large number of e-folds of inflation.

5 Conclusions

In this article we have investigated in detail the consequences of the scalar-tensor model of DBI inflation introduced in [27], paying particular attention to the effect of the different parameters on the value of the spectral index. When the coupling between the two fields is non-zero, the φ -field (with a canonical kinetic term in its Lagrangian) is forced into the minimum of its effective potential. Although it does not play a dynamical role, the field indirectly affects the DBI field χ and the perturbations via the conformal coupling factor

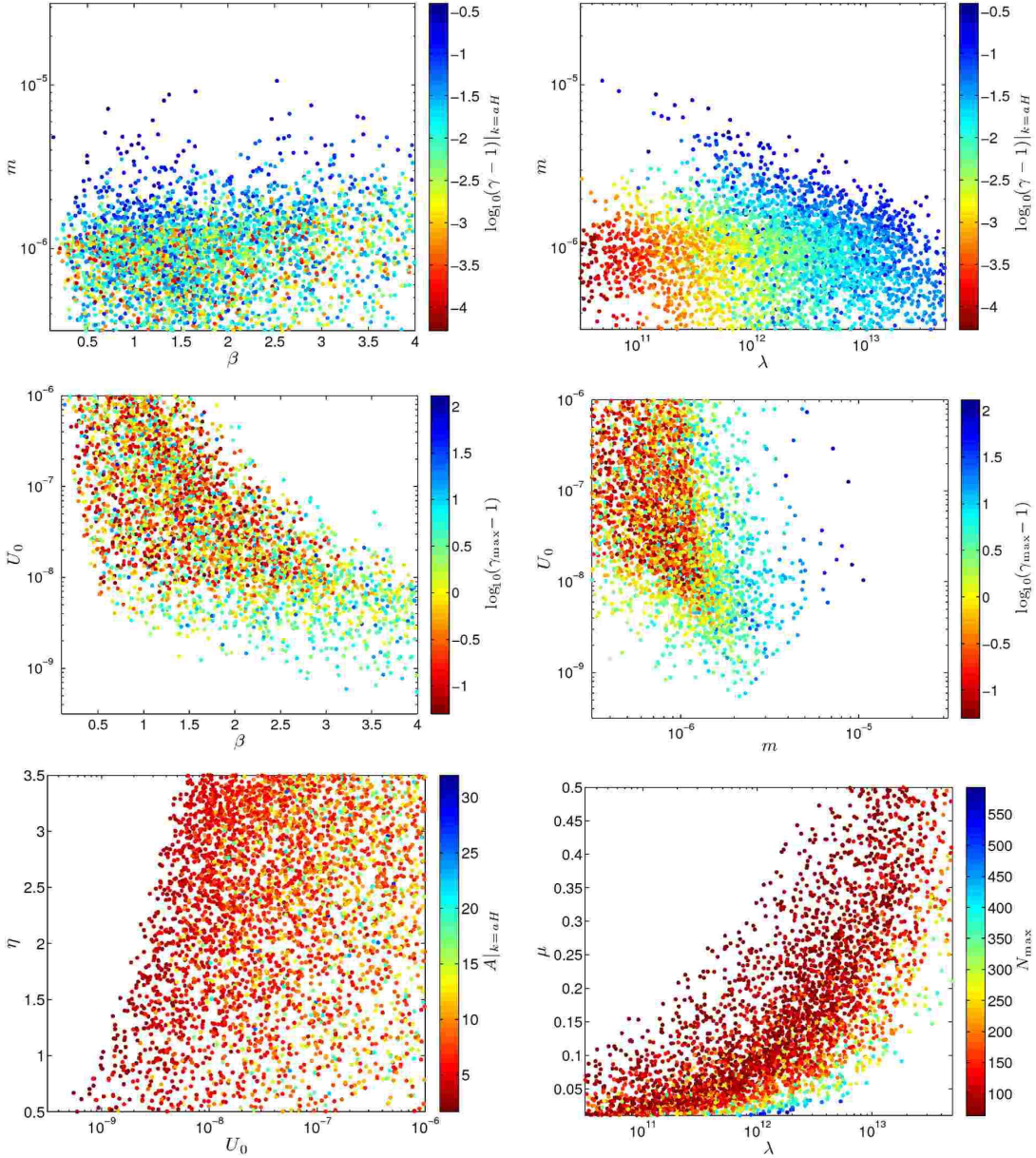


Figure 5. Views of the parameter space for the ‘best set’ (for which the calculated values of n_s and P_{amp} are within observational limits) for the exponential potential. Top row: the $\beta - \log_{10} m$ (left) and $\log_{10} \lambda - \log_{10} m$ (right) planes, colour-coded according to the value of $\log_{10}(\gamma - 1)$ at $k_{\text{pivot}} = aH$. Middle row: the $\beta - \log_{10} U_0$ (left) and $\log_{10} m - \log_{10} U_0$ (right) planes, colour-coded according to the value of $\log_{10}(\gamma_{\text{max}} - 1)$. The bottom row shows the $\log_{10} U_0 - \eta$ plane, colour-coded according to the value of A at $k_{\text{pivot}} = aH$, and the $\log_{10} \lambda - \mu$ plane, colour-coded according to the value of N_{max} .

$A = \exp(\beta\varphi)$. With the φ -field in its minimum and working in the ‘slow-roll limit’ in which the equation of motion for the DBI field is dominated by the potential $V(\chi)$ (with effective mass mA) we have shown that, with appropriate slow-roll parameters, the perturbation equations can be put in a form similar to that describing perturbations in single-field k-

inflation, with an additional small correction due to the two-field nature of the full system. In the limit that this can be neglected, the resulting estimate for the spectral index is

$$n_s = 1 - 2s + 2\delta - 6\epsilon \left(1 + \frac{2\beta}{\eta}\right),$$

which is superficially similar to the standard expressions for the single field DBI scenario. However, the ϵ and δ parameters are proportional to $A^{-2} (1 + 4\beta/\eta)^{-2}$ and $A^{-2} (1 + 4\beta/\eta)^{-1}$ respectively, so tend to be smaller than their counterparts in the uncoupled case (with all other parameters unchanged). The values of the slow-roll parameters, are dependent on the background evolution of the fields (which in turn are determined by quantities such as the mass of the DBI field) and the actual value of the n_s can exhibit either a blue- or red-tilt.

Understanding the effect of the free parameters of the model on the observable quantities is essential: the numerical work described in Sec. 4 represents a first step toward this end. It is shown that the parameter space can be severely constrained by the requirement that the mechanism must be capable of driving a sufficient amount of inflation and by considering the values of the power spectrum amplitude and the spectral index. The latter measurement in particular rules out a large class of models — those with small values of c_s at horizon crossing, which give rise to a blue-tilted spectrum — so that only scenarios in which DBI characteristics are suppressed at the beginning of the observable period of inflation are allowed. In general, the excluded models with $(\gamma - 1) \gtrsim \mathcal{O}(1)$ at horizon crossing exhibit significant DBI effects (i.e. large values of the boost factor) throughout the inflationary period. The remaining realisations of the model have $(\gamma - 1) \ll 1$ at horizon crossing: some of which differ only slightly from standard slow-roll solutions. This is in general agreement with the results of other numerical studies investigating the standard DBI model [5] where it was found that only models exhibiting small DBI effects were viable. However, a number of viable cases — associated with a more red-tilted spectral index — were found for which the boost factor is initially suppressed by the effect of the coupling between the fields, but increases later to moderate values $\sim \mathcal{O}(10)$. Further work is needed to fully understand the viability of the model; a natural extension is to consider other observables: in particular, the tensor-to-scalar ratio r and the level of non-Gaussianity (proportional to γ^2 in the single-field case) which so tightly constrains the standard DBI scenario. It would also be of interest to calculate the running of the spectral index, as including this gives different bounds on the spectral index [34].

In conclusion, the scalar-tensor DBI inflation scenario provides a simple mechanism to reduce the large values of the boost factor associated with single field models with DBI action, whilst still being able to drive 60 e-folds of inflation. We have indicated the regions of the parameter space of the model capable of giving rise to a power spectrum with amplitude and spectral index within the observed bounds, and moreover shown analytically that the value of the latter quantity arises when the coupling forces one field into its minimum, leaving the DBI field to slow-roll.

Acknowledgments

D.F.M. thanks the Research Council of Norway FRINAT grant 197251/V30. D.F.M. is also partially supported by project PTDC/FIS/111725/2009 and CERN/FP/116398/2010. J.M.W. was supported by Yggdrasil Grant 195757/V11 from the research council of Norway, and would like to thank the members of the Institute of Theoretical Astrophysics at the

University of Norway for their kind hospitality while this work was initiated. We would also like to thank the anonymous referee for helpful and constructive comments.

A Approximating $C_{\chi\chi}$ to first order in slow-roll parameters

In this appendix, we derive an first-order expression for the mass term $C_{\chi\chi}$ [given in full by (3.15)] that appears in the perturbed equation of motion (3.14). Before rewriting each contribution to this equation in terms of the slow roll parameters ϵ , δ and s , it is necessary to obtain an expression involving f_χ . To do this, one can differentiate $(1 - c_s^2) = A^{-2}f\dot{\chi}^2$ to get a relation between $\ddot{\chi}$ and f_χ . This yields

$$\frac{\ddot{\chi}}{\dot{\chi}} = \beta\dot{\phi} - \frac{1}{2}\frac{f_\chi}{f}\dot{\chi} + (1 - c_s^{-2})^{-1}\frac{\dot{c}_s}{c_s}, \quad (\text{A.1})$$

$$\Rightarrow \frac{\ddot{\chi}}{H\dot{\chi}} \simeq \frac{2\beta}{\eta}\epsilon - \frac{1}{2}\frac{f_\chi}{f}\frac{\dot{\chi}}{H} + (1 - c_s^{-2})^{-1}s. \quad (\text{A.2})$$

Then differentiate $-2\dot{H} \simeq A^2\gamma\dot{\chi}^2$ to obtain,

$$\begin{aligned} 2\dot{\epsilon}H^2 + 4\epsilon H\dot{H} &\simeq (2\beta\dot{\phi} - \dot{c}_s/c_s)(2\epsilon H^2) + 2A^2\gamma\dot{\chi}\ddot{\chi}, \\ \frac{\dot{\epsilon}}{2H\epsilon} - \epsilon &\simeq \frac{2\beta}{\eta}\epsilon - \frac{1}{2}s + \frac{\ddot{\chi}}{H\dot{\chi}}. \end{aligned} \quad (\text{A.3})$$

Substituting (3.11) and (A.2) gives

$$-\frac{1}{2}\frac{f_\chi}{f}\frac{\dot{\chi}}{H} \simeq (1 - c_s^2)^{-1}s - \delta + \left(1 + \frac{2\beta}{\eta}\right)\epsilon. \quad (\text{A.4})$$

We can now write each contribution to $C_{\chi\chi}$ in (3.15) in terms of the slow roll parameters ϵ , δ and s , working to $\mathcal{O}(\epsilon)$ and dropping second order terms. Starting at the beginning

- The first term is

$$\begin{aligned} \frac{A^4\dot{\chi}}{H}\frac{f_\chi}{f^2}(1 - c_s)^2 &= -2A^2\dot{\chi}^2\left(\frac{1 - c_s}{1 + c_s}\right)\left[-\frac{1}{2}\frac{f_\chi}{f}\frac{\dot{\chi}}{H}\right], \\ &\simeq -4c_s\epsilon H^2\left(\frac{1 - c_s}{1 + c_s}\right)\left[-\frac{1}{2}\frac{f_\chi}{f}\frac{\dot{\chi}}{H}\right], \\ &\simeq -4c_s\epsilon H^2\left(\frac{1 - c_s}{1 + c_s}\right)\left[(1 - c_s^2)^{-1}s - \delta + \left(1 + \frac{2\beta}{\eta}\right)\epsilon\right], \\ &\sim \mathcal{O}(\epsilon^2 H^2). \end{aligned}$$

using $A^2\gamma\dot{\chi}^2 \simeq 2\epsilon H^2$.

- The second term is

$$\begin{aligned} -\left[\frac{f_\chi}{f} - \frac{A^2\dot{\chi}}{Hc_s}\right]\frac{\dot{c}_s}{c_s}\dot{\chi} &= \left[-\frac{f_\chi}{f}\frac{\dot{\chi}}{H} + \frac{A^2\gamma\dot{\chi}^2}{H^2}\right]\left(\frac{\dot{c}_s}{Hc_s}\right)H^2, \\ &\simeq \left[2(1 - c_s^2)^{-1}s - 2\delta + 4\left(1 + \frac{\beta}{\eta}\right)\epsilon\right]sH^2, \\ &\sim \mathcal{O}(\epsilon^2 H^2). \end{aligned}$$

- The third term is

$$\begin{aligned}
-\frac{1}{2}c_s f_\chi A^{-4} \dot{\chi}^2 V_{T,\chi} &= -\frac{1}{2}c_s f_\chi \dot{\chi}^2 V_\chi \\
&= \frac{1}{2} \frac{f_\chi}{Hf} (1 - c_s^2) (-A^2 c_s V_\chi) H \\
&\simeq 3H^2 (1 - c_s^2) \left[\frac{1}{2} \frac{f_\chi \dot{\chi}}{Hf} \right] \\
&\simeq 3H^2 \left[(1 - c_s^2) \delta - s - (1 - c_s^2) \left(1 + \frac{2\beta}{\eta} \right) \epsilon \right] \quad (\text{A.5})
\end{aligned}$$

where (3.7) was used in the third step and (A.4) in the last.

- The fourth term is

$$\frac{1}{2} A^2 (1 - c_s)^2 \left[c_s \left(\frac{f_\chi}{f^2} \right)_{,\chi} + (1 + c_s) f^{-1} \left(\frac{f_\chi}{f} \right)_{,\chi} \right] = \frac{1 - c_s}{2(1 + c_s)} \left[(1 + 2c_s) - c_s \left(\frac{f_\chi}{f} \right) \right] \left(\frac{f_\chi}{f} \right)_{,\chi} \dot{\chi}^2.$$

The final part of this term can be expressed in terms of time derivatives of the slow-roll parameters and other second-order terms

$$\begin{aligned}
\frac{1}{2} \left(\frac{f_\chi}{f} \right)_{,\chi} \dot{\chi}^2 &= \left(\frac{f_\chi \dot{\chi}}{2f} \right) \cdot - \frac{1}{2} \frac{f_\chi}{f} \ddot{\chi}, \\
&= H \left(\frac{f_\chi \dot{\chi}}{2Hf} \right) \cdot + H^2 \left(\frac{f_\chi \dot{\chi}}{2Hf} \right) \left(\epsilon - \frac{\ddot{\chi}}{H\dot{\chi}} \right) \\
&\sim \mathcal{O}(H^2 \epsilon^2), \quad (\text{A.6})
\end{aligned}$$

using (A.4) and (A.2). We have checked numerically to confirm that the contribution of this term to $C_{\chi\chi}$ is negligible.

- The fifth term is

$$\frac{3}{2} A^2 \dot{\chi}^2 c_s^{-1} (1 + c_s^2) \simeq 3H^2 (1 + c_s^2) \epsilon. \quad (\text{A.7})$$

- The sixth term is

$$-A^4 c_s^{-2} \frac{\dot{\chi}^4}{2H^2} \simeq 2H^2 \epsilon^2 \sim \mathcal{O}(\epsilon^2 H^2).$$

- The seventh term is

$$-A^2 c_s^{-1} (1 + c_s^2) \frac{\dot{\chi}^2 \dot{\varphi}^2}{4H^2} \simeq -\frac{2}{\eta^2} (1 + c_s^2) H^2 \epsilon^3 \sim \mathcal{O}(\epsilon^3 H^2).$$

using (3.10).

- The eighth term is

$$\begin{aligned}
\frac{\dot{\chi} V_{T,\chi}}{H} (1 + c_s^2) &\simeq -(1 + c_s^2) \frac{A^6 V_\chi^2}{3\gamma H^2}, \\
&\simeq -3H^2 (1 + c_s^2) \left[\frac{1}{A^2 \gamma} \left(1 + \frac{4\beta}{\eta} \right)^{-2} \frac{V_\chi^2}{V^2} \right], \\
&\simeq -6H^2 (1 + c_s^2) \epsilon. \quad (\text{A.8})
\end{aligned}$$

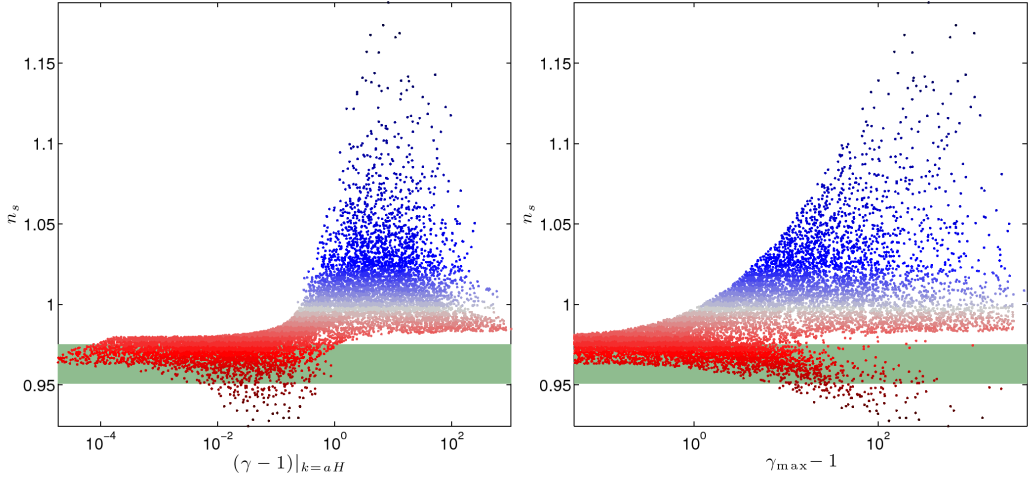


Figure 6. The distribution of $(\gamma - 1)$ values for the offset quadratic potential. Quantities plotted are the same as in fig. 3.

- The final term is

$$\begin{aligned}
 c_s^3 A^{-2} V_{T,\chi\chi} &= c_s^3 A^2 V_{\chi\chi}, \\
 &= 3H^2 c_s^2 \left[\frac{1}{A^2 \gamma} \left(1 + \frac{4\beta}{\eta}\right)^{-1} \frac{V_{\chi\chi}}{V} \right], \\
 &= 3H^2 c_s^2 \delta.
 \end{aligned} \tag{A.9}$$

Combining eqns. (A.5), (A.7), (A.8) and (A.9) then gives eqn. (3.16)

$$C_{\chi\chi} \simeq 3H^2 \left(\delta - s - 2\epsilon \left[1 + \frac{\beta}{\eta} (1 - c_s^2) \right] \right).$$

B Comparing the exponential and quadratic potentials

As mentioned in the body of the article, the numerical analysis in Sec. 4 was repeated with an offset quadratic potential for φ -field (as described in [27]) given by

$$U(\varphi) = U_0(\varphi - \eta)^2. \tag{B.1}$$

Like the exponential potential, this is dependent on two free parameters U_0 and η : in this case the latter gives the value of the true minimum is $\varphi = \eta$. The parameter ranges were

$$\begin{aligned}
 \beta &\in [0.1, 4], \quad \lambda \in [10^{10.5}, 5 \times 10^{14}], \quad m \in [10^{-6.5}, 10^{-4.5}], \\
 U_0 &\in [10^{-11}, 10^{-7}], \quad \mu \in [0.01, 0.5], \quad \eta \in [1, 6].
 \end{aligned} \tag{B.2}$$

Again, 5 million parameter sets were investigated, of which 2,748,236 (55.0%) satisfied the criteria for the background evolution. As with the exponential potential, of the points rejected at this stage, most (56%) yielded too few efolds, with the majority of the remainder exhibiting slow-roll in χ (41%). 11,999 of the acceptable parameter sets had a power spectrum amplitude

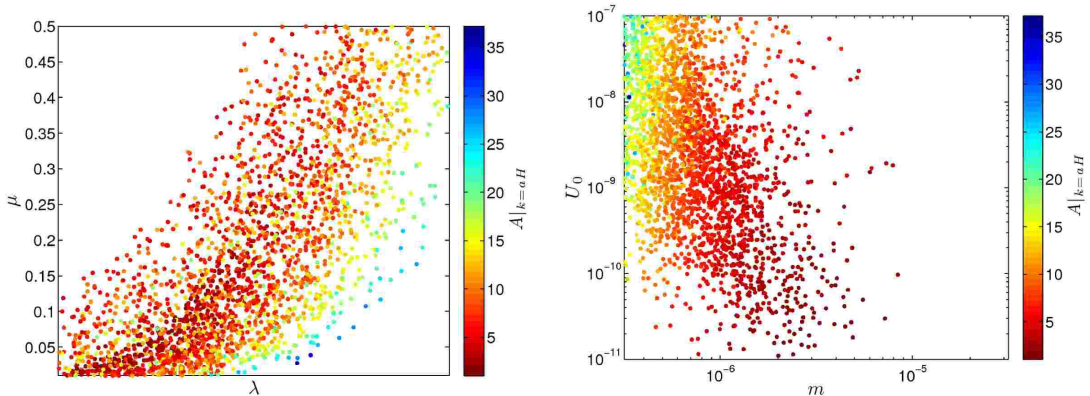


Figure 7. Two views of the parameter space for the ‘best set’ (for which the calculated values of n_s and P_{amp} are within observational limits) for the quadratic potential, colour-coded according to the value of A at $k_{\text{pivot}} = aH$. Left panel: $\log_{10} \lambda - \mu$; right panel: $\log_{10} m - \log_{10} U_0$.

within the observed range, and the ‘best’ set (for which both the power spectrum and spectral index were within observational limits) yielded 2548 points.

The parameter space for the quadratic potential is very similar to that of the exponential potential in many respects, with the exception of those involving the parameter η , which has a different interpretation in each case. For example, for the exponential potential smaller values of η give rise to larger values of the power spectrum amplitude, due to the increase in size of the potential $U(\varphi)$. For the quadratic potential, for the same reason, it is larger values of η that are correlated with P_{amp} . Focusing on the parameter space for the ‘better’ set for this potential consisting of parameters that give rise to P_{amp} within observational limits, it is again possible to identify two groups of points in the parameter space. The interpretation is the same as in the case of the exponential potential: runs that deviate significantly from quasi-slow-roll behaviour (i.e. $(\gamma - 1) \ll 1$) as the pivot mode leaves the horizon give rise to a blue-tilted spectrum with $n_s > 1$ (blue points) and runs in which DBI characteristics are suppressed at $N = 55$, but become significant later during inflation, exhibit a strong red-tilt (dark red points). The similarity between the two potentials can be seen by comparing figs. 3 and 6, which show the correlation between the spectral index and the boost factor.

Looking at the ‘best’ set, with both the power spectrum amplitude and spectral index satisfying observational constraints, we see more similarities between the results for the quadratic and exponential potentials. The distribution of points in the views of the parameter space showing the mass parameters and the warp factor parameters shown in fig. 7 are almost identical to those for the exponential potential (cf. middle-right and bottom-right plots in fig. 5). Again, there is a strong correlation between small values of the DBI mass and large values of the coupling A (and also large values of N_{max}).

The general distribution of the points in the parameter space is largely the same for both potentials although the β dependence is a little different. For the exponential potential, the set of allowed parameters is cut off abruptly in the $\beta - \log_{10} U_0$ plane (see in the left-hand plots in fig. 4) when β and U_0 are large as the Hubble scale (and by extension, P_{amp}) becomes too large. In the equivalent plot for the quadratic potential (not shown) H depends also on the displacement of the field from its true minimum, and so the effect of U_0 and β is modulated by other parameters and the cutoff is not so clear.

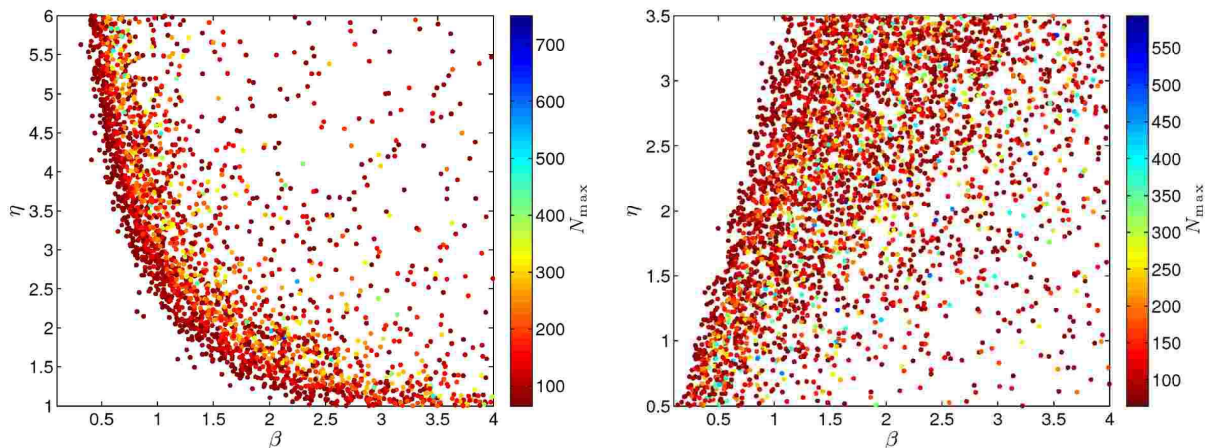


Figure 8. The $\beta - \eta$ planes for the quadratic potential (left) and the exponential potential (right), using the ‘best sets’. Both plots are colour-coded according to the value of N_{\max} (cf. analytical constraints shown in fig. 9).

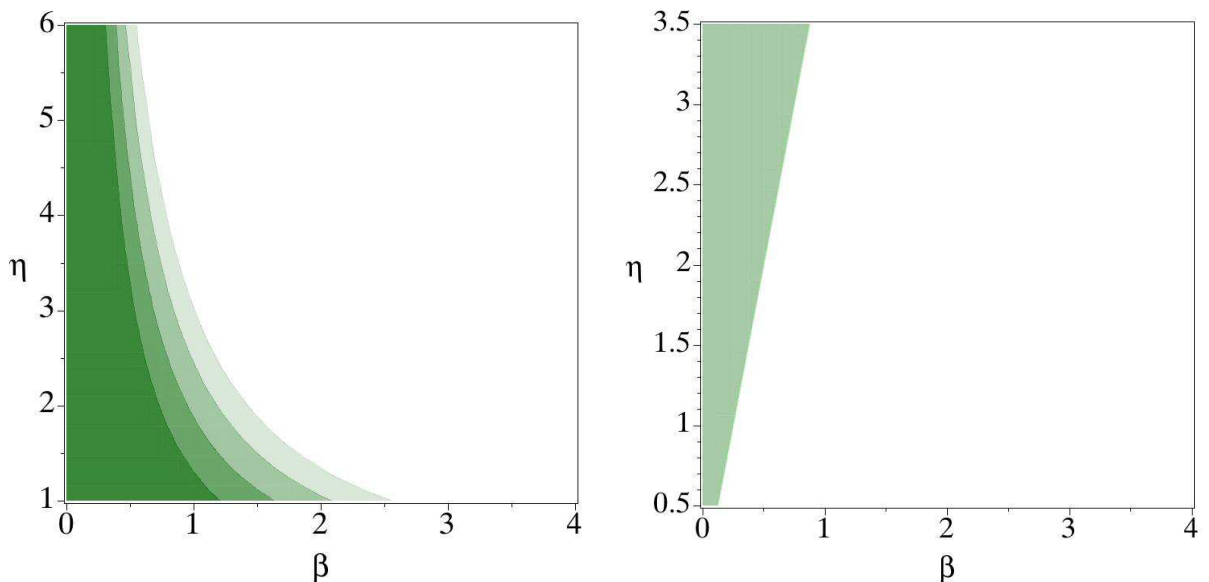


Figure 9. For comparison with fig. 8, the shaded regions show the regions of the $\eta - \beta$ planes in which the condition $\rho_{\text{DBI}} > \rho_\varphi$ is satisfied for the quadratic (left panel) and exponential potentials (right panel) using the same parameter ranges. The former condition is dependent on the ratio V/U_0 (see text) so we have used $V/U_0 = 10^{-5}, 10^{-4}, 10^{-3}, 10^{-2}$, with the lightest shade corresponding to 10^{-5} .

We have remarked that the differences between the observationally viable regions of the parameter spaces for the exponential and quadratic potentials are manifest when the parameters β and η are plotted. It is interesting to compare the plots in fig. 7 with those in fig. 9, representing the constraints derived analytically (in [27]) under the assumption that the fields are dominated by their potential terms. As shown in [27] the condition $\rho_{\text{DBI}} > \rho_\varphi$

is given by $W(x \approx 8\beta^2 V e^{4\beta\eta}/U_0) < 2$ in terms of Lambert's W function for the quadratic potential and $\eta > 4\beta$ for the exponential potential. It can be seen that the areas in fig. 8 that correspond to the shaded regions in fig. 9 — in which the DBI energy density is dominant — are almost completely devoid of points. Also, many of the points are clustered in the vicinity of the $\rho_{\text{DBI}} = \rho_\varphi$ boundary. Thus, in the majority of runs with parameters that give rise to a power spectrum with a spectral index within observable limits, the energy density of the DBI field is a subdominant but non-negligible fraction of the total energy density.

References

- [1] E. Silverstein and D. Tong, *Scalar Speed Limits and Cosmology: Acceleration from D-acceleration*, *Phys. Rev.* **D70** (2004) 103505, [[hep-th/0310221](#)].
- [2] M. Alishahiha, E. Silverstein, and D. Tong, *DBI in the sky*, *Phys. Rev.* **D70** (2004) 123505, [[hep-th/0404084](#)].
- [3] C. Armendariz-Picon, T. Damour, and V. F. Mukhanov, *k-Inflation*, *Phys. Lett.* **B458** (1999) 209–218, [[hep-th/9904075](#)].
- [4] J. Garriga and V. F. Mukhanov, *Perturbations in k-inflation*, *Phys. Lett.* **B458** (1999) 219–225, [[hep-th/9904176](#)].
- [5] R. Bean, S. E. Shandera, S. H. Henry Tye, and J. Xu, *Comparing Brane Inflation to WMAP*, *JCAP* **0705** (2007) 004, [[hep-th/0702107](#)].
- [6] H. V. Peiris, D. Baumann, B. Friedman, and A. Cooray, *Phenomenology of D-Brane Inflation with General Speed of Sound*, *Phys. Rev.* **D76** (2007) 103517, [[arXiv:0706.1240](#)].
- [7] D. Baumann and L. McAllister, *A Microscopic Limit on Gravitational Waves from D-brane Inflation*, *Phys. Rev.* **D75** (2007) 123508, [[hep-th/0610285](#)].
- [8] L. Lorenz, J. Martin, and C. Ringeval, *Constraints on Kinetically Modified Inflation from WMAP5*, *Phys.Rev.* **D78** (2008) 063543, [[arXiv:0807.2414](#)].
- [9] L. Lorenz, J. Martin, and C. Ringeval, *K-inflationary Power Spectra in the Uniform Approximation*, *Phys.Rev.* **D78** (2008) 083513, [[arXiv:0807.3037](#)].
- [10] J. E. Lidsey and I. Huston, *Gravitational wave constraints on Dirac-Born-Infeld inflation*, *JCAP* **0707** (2007) 002, [[arXiv:0705.0240](#)].
- [11] M. Spalinski, *A consistency relation for power law inflation in DBI models*, *Phys. Lett.* **B650** (2007) 313–316, [[hep-th/0703248](#)].
- [12] D. A. Easson, R. Gregory, D. F. Mota, G. Tasinato, and I. Zavala, *Spinflation*, *JCAP* **0802** (2008) 010, [[arXiv:0709.2666](#)].
- [13] R. Gregory and D. Kaviani, *Spinflation with Angular Potentials*, [[arXiv:1107.5522](#)].
- [14] D. Langlois, S. Renaux-Petel, D. A. Steer, and T. Tanaka, *Primordial fluctuations and non-Gaussianities in multi-field DBI inflation*, *Phys. Rev. Lett.* **101** (2008) 061301, [[arXiv:0804.3139](#)].
- [15] D. Langlois, S. Renaux-Petel, D. A. Steer, and T. Tanaka, *Primordial perturbations and non-Gaussianities in DBI and general multi-field inflation*, *Phys. Rev.* **D78** (2008) 063523, [[arXiv:0806.0336](#)].
- [16] S. Mizuno, F. Arroja, K. Koyama, and T. Tanaka, *Lorentz boost and non-Gaussianity in multi-field DBI-inflation*, *Phys. Rev.* **D80** (2009) 023530, [[arXiv:0905.4557](#)].
- [17] S. Mizuno, F. Arroja, and K. Koyama, *On the full trispectrum in multi-field DBI inflation*, *Phys.Rev.* **D80** (2009) 083517, [[arXiv:0907.2439](#)].

- [18] C. Burgess, R. Easther, A. Mazumdar, D. F. Mota, and T. Multamaki, *Multiple inflation, cosmic string networks and the string landscape*, *JHEP* **0505** (2005) 067, [[hep-th/0501125](#)].
- [19] S. Renaux-Petel, *Combined local and equilateral non-Gaussianities from multifield DBI inflation*, *JCAP* **0910** (2009) 012, [[arXiv:0907.2476](#)].
- [20] D. Langlois, S. Renaux-Petel, and D. A. Steer, *Multi-field DBI inflation: Introducing bulk forms and revisiting the gravitational wave constraints*, *JCAP* **0904** (2009) 021, [[arXiv:0902.2941](#)].
- [21] Y.-F. Cai and H.-Y. Xia, *Inflation with multiple sound speeds: a model of multiple DBI type actions and non-Gaussianities*, *Phys. Lett.* **B677** (2009) 226–234, [[arXiv:0904.0062](#)].
- [22] L. P. Chimento, R. Lazkoz, and M. G. Richarte, *Enhanced Inflation in the Dirac-Born-Infeld framework*, *Phys.Rev.* **D83** (2011) 063505, [[arXiv:1011.2345](#)].
- [23] D. A. Easson and R. Gregory, *Circumventing the eta problem in building an inflationary model in string theory*, *Phys. Rev.* **D80** (2009) 083518, [[arXiv:0902.1798](#)].
- [24] D. A. Easson, S. Mukohyama, and B. A. Powell, *Observational Signatures of Gravitational Couplings in DBI Inflation*, *Phys. Rev.* **D81** (2010) 023512, [[arXiv:0910.1353](#)].
- [25] P. Brax and E. Cluzel, *Brane Bremsstrahlung in DBI Inflation*, *JCAP* **1003** (2010) 016, [[arXiv:0912.0806](#)].
- [26] P. Brax and E. Cluzel, *Perturbation Theory in k-Inflation Coupled to Matter*, *JCAP* **1104** (2011) 014, [[arXiv:1102.1917](#)].
- [27] C. van de Bruck, D. F. Mota, and J. M. Weller, *Embedding DBI inflation in scalar-tensor theory*, *JCAP* **1103** (2011) 034, [[arXiv:1012.1567](#)].
- [28] P. Brax, C. van de Bruck, L. M. Hall, and J. M. Weller, *Slow-Roll Inflation in the Presence of a Dark Energy Coupling*, *Phys.Rev.* **D79** (2009) 103508, [[arXiv:0812.2843](#)].
- [29] S. Kecskemeti, J. Maiden, G. Shiu, and B. Underwood, *DBI inflation in the tip region of a warped throat*, *JHEP* **09** (2006) 076, [[hep-th/0605189](#)].
- [30] K. Tzirakis and W. H. Kinney, *Non-canonical generalizations of slow-roll inflation models*, *JCAP* **0901** (2009) 028, [[arXiv:0810.0270](#)].
- [31] C. Ringeval, *Dirac-Born-Infeld and k-inflation: the CMB anisotropies from string theory*, *J.Phys.Conf.Ser.* **203** (2010) 012056, [[arXiv:0910.2167](#)]. * Brief entry *.
- [32] M. Abramowitz and I. A. Stegun, *Handbook of Mathematical Functions with Formulas, Graphs, and Mathematical Tables*. Dover, New York, ninth dover printing, tenth gpo printing ed., 1965.
- [33] A. R. Liddle and D. H. Lyth, *Cosmological Inflation and Large-Scale Structure*. Cambridge University Press, 2006.
- [34] **WMAP Collaboration** Collaboration, E. Komatsu *et. al.*, *Seven-Year Wilkinson Microwave Anisotropy Probe (WMAP) Observations: Cosmological Interpretation*, *Astrophys.J.Suppl.* **192** (2011) 18, [[arXiv:1001.4538](#)].